Journal of Power Sources 241 (2013) 127–135

Contents lists available at SciVerse ScienceDirect

Journal of Power Sources

journal homepage: www.elsevier.com/locate/jpowsour

Position dependent analysis of membrane electrode assembly degradation of a direct methanol fuel cell via electrochemical impedance spectroscopy

Peter Hartmann, Nada Zamel, Dietmar Gerteisen*

Fraunhofer Institute for Solar Energy Systems, Freiburg, Germany

HIGHLIGHTS

- Local degradation of a long-term operated DMFC MEA is analyzed.
- Anode and cathode impedance are measured by reference electrode.
- Anode spectra were analyzed by equivalent circuit modeling.
- Degradation is not correlated with the flow field pattern.

ARTICLE INFO

Article history:
Received 13 July 2012
Received in revised form
25 March 2013
Accepted 7 April 2013
Available online 29 April 2013

Keywords:
Degradation
DMFC
Electrochemical impedance spectroscopy
Spatial influence

ABSTRACT

The performance of a direct methanol fuel cell MEA degraded during an operational period of more than 3000 h in a stack is locally examined using electrochemical impedance spectroscopy. Therefore, after disassembling the MEA is cut into small pieces and analyzed in a 1 cm^2 test cell. Using a reference electrode, we were capable of measuring the anode and cathode spectra separately. The spectra of the segments at different positions do not follow a specified trend from methanol inlet to outlet of the stack flow field. The anode spectra were analyzed with an equivalent circuit simulation. The conductance of the charge transfer was found to increase with current density up to a point where a raising limitation process of the complex methanol oxidation dominates, which is not a bottleneck at low current density. Further, an increase of the double layer capacitance with current density was observed. The diffusion resistance was calculated as an effective diffusion coefficient in the order of 10^{-10} m^2 s^{-1}; implying that the diffusion limitation is not the bulk diffusion in the backing layer. Finally, the degree of poisoning of the catalysts by carbon monoxide was measured as a pseudo inductive arc and decreases with increasing current.

1. Introduction

With rising interest in the operation of direct methanol fuel cells (DMFC), understanding the reaction kinetics, transport phenomena and their respective limitations in these cells is important. This is especially significant for the electrodes and the electrolyte membrane. As is the case with many electrochemical devices, electrochemical impedance spectroscopy (EIS) is often employed to investigate these phenomena. For these measurements, a small harmonic interference is introduced to the system at steady state as a sinusoidal signal, $i_{AC}(t) = \hat{i}\sin(\omega t)$, with the resulting voltage response, $V_{AC}(t) = \hat{V}\sin(\omega t + \varphi)$. The complex impedance of the cell can thus be determined from the perturbation and response signals as follows:

$$Z(\omega) = \frac{\int V_{AC}(t)\mathrm{d}t}{\int i_{AC}(t)\mathrm{d}t} \quad (1)$$

Much work is found in the literature focusing on the investigation of the faradaic impedance of DMFC anodes as well as the degradation of the cell. Müller et al. [1] examined the kinetics and the mechanism of methanol electro-oxidation by measuring the impedance of the anodes in a hydrogen/methanol cell configuration and operating without mass-transport limitations. Upon the exclusion of such limitations, they measured inductive loops in the complex plane at low frequencies. They attributed such loops to the reaction mechanism for methanol electro-oxidation. This conclusion was also supported by a simple equivalent circuit. The methanol oxidation on platinum electrodes was also studied experimentally and

* Corresponding author.
E-mail address: Dietmar.gerteisen@ise.fraunhofer.de (D. Gerteisen).

0378-7753/$ – see front matter © 2013 Elsevier B.V. All rights reserved.
http://dx.doi.org/10.1016/j.jpowsour.2013.04.041

numerically by Seland et al. [2]. Their electrochemical impedance spectra were calculated from voltammograms at frequencies from 20 kHz to 0.5 Hz. With this type of measurement, steady state conditions are avoided; thus, transient effects such as partial coverage of CO onto the platinum can be studied. From their measurements, Seland et al. [2] proposed that the rate-determining step on a platinum catalyst is the reaction of adsorbed CO and OH and the competition between these two species. EIS can also be used to analyze the reaction kinetics and interfacial characteristics of the anode as has been done in Ref. [3]. Hsu et al. [3] modeled the spectra of DMFC anode with the incorporation of the constant phase element (CPE) at the interface of the anode catalyst layer and membrane. From their results, they too observed an inductive behavior at low frequencies attributed to methanol electro-oxidation. The effect of methanol crossover on the performance of DMFCs was measured with EIS in Ref. [4] and found to result in a decrease in the charge transfer resistance. The oxidation of CO on platinum in a micro DMFC was studied using EIS measurements by Schulz et al. [5]. They found that the performance of the cell was governed by the presence of CO in the anode. Finally, electrochemical impedance spectroscopy has also been used to understand DMFC degradation. In Ref. [6], Park et al. studied the effect of on/off cycling on the performance of DMFC. They found that the cycling of voltage resulted in degradation more severe than that of continuous voltage and current operation. This was observed in their EIS measurements, where the charge transfer resistance was increased with voltage cycling.

In this study, we use electrochemical impedance spectroscopy to investigate the effects of degradation on the overall performance of DMFC membrane electrode assembly (MEA). This study is unique in that the MEA aging process occurs during operation in a forklift. This aging process allows us to understand the effect of "real life" degradation and its overall influence on the performance of the cell. This analysis is carried out for six segments on different positions of the stack MEA; hence, to investigate the impact of all inhomogeneities on degradation. Further, in this study, we carry out the impedance measurements using an air/methanol configuration with a reference electrode inside the cathode flow compartment. With this type of analysis, we are able to separate the anode and cathode spectra. Finally, an equivalent circuit model is used to complement our measurements and to further our understanding of the degradation mechanisms, which have taken place.

2. Investigation techniques

2.1. Experimental

EIS measurements are based on the linear response theory given in Ref. [7]. According to this theory, the system response to an interfering signal is linear. Since the electrochemical systems have a strong non-linear behavior, it is important to select a small amplitude of an interfering signal, $\hat{i}$, so that the nonlinear effects can be neglected [7]. In this study, we use an excitation current within 5% of the DC signal [8]. The impedance measurements are carried out at a specific point on the polarization curve. In this study, our measurements are carried out at three different current densities, 50, 150 and 250 mA cm^{-2}. At steady-state to capture the relevant transport and electrochemical process taking place a DMFC, we perform the impedance measurements over a frequency range of 10 kHz to 0.05 Hz with 7 points per decade.

In this study, we measure EIS of an aged MEA at different positions to investigate the degradation caused by local inhomegeneities during the stack operation. The MEA under study was obtained from a stack consisting of 90 cells and have been operated for more than 3000 h under various start up and shut down conditions. The MEA has an active area of 320 cm^2 with a Nafion 115 as the membrane, Pt–Ru anode catalyst with a loading of 3.0 mg Pt cm^{-2} and 1.5 mg Ru cm^{-2} and Pt cathode catalyst with a loading of 1.5 mg cm^{-2}. A microporous layer is sandwiched between the catalyst layer and the gas diffusion layer on both the anode and cathode sides. The stack MEA was segmented as shown in Fig. 1. In this study, we investigate the degradation of the segments 2, 5, 8, 11, 14, and 17, which are related to the flow field pattern, where the stack was operated in counter-flow mode. From each segment, we obtained a 1 cm^2 active area to create a test cell. By means of Laser ablation technique a 300 μm wide gap is simultaneously implemented on both electrodes, anode and cathode. This results in an electrically isolated part on the electrodes within the reactant compartment, which serve as reference electrodes. Details of the used test cell, test bench and the use of Laser ablation technique for preparing reference electrodes are given in Gerteisen [9]. In other words, the EIS measurements were run for each segment as a stand alone cell. These measurements were obtained using Solartron 1255 HF Frequency Response Analyzer combined with a Solartron 1286 Electrochemical Interface and adhere to the measurement conditions listed in Table 1. The cell is run at each condition for 30 min to ensure that steady state condition is reached before collecting any spectrum. Each spectrum has also been measured twice to ensure the repeatability of the measurements.

2.2. Equivalent circuit modeling

In order to further investigate the trends observed experimentally, the anode spectra are analyzed mathematically using the simulation program ZView™. The closely coupled physical and chemical processes in the anode can be simplified to a cylindrical pore model in series with a Warburg diffusion element and both are in parallel with an inductance combined with an ohmic resistor as shown in Fig. 2a. In this model, we consider four variations as explained in Fig. 2b. Each variation depends on the overall current density of the cell and is used to capture each characteristic of the measured spectra. As evident from the SEM images shown in our previous study [10], the pore distribution of the electrode can vary in distribution; hence, the methanol and water diffusing through the porous electrode will also vary before the methanol is oxidized at the three-phase interface. This difference in distribution is also affected by the thickness of the electrodes. From our measurements, we found that a typical thickness of the porous electrode

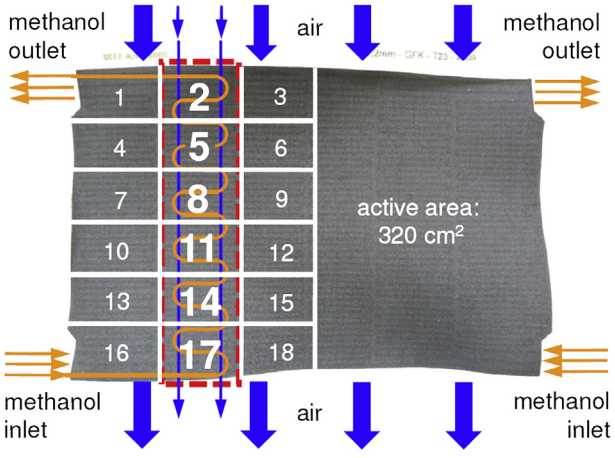

Fig. 1. Examined aged MEAs with an impression of the flow filed – characterized segments (2, 5, 8, 11, 14, 17) highlighted in red – a parallel flow field is used for air – a serpentine flow field is used for methanol. (For interpretation of the references to color in this figure legend, the reader is referred to the web version of this article.)

Table 1
Operating conditions of the test cells.

Concentration of the methanol–water-solution	1	M
Volume flow of the methanol–water-solution	0.8	ml min^{-1}
Volume flow of the air	37	ml min^{-1}
Pressure at the cathode	1150	mbar
Cell temperature	70	°C
Temperature of the inlet tube at the cathode side	70	°C
Temperature of the outlet tube at the cathode side	75	°C
Dew point of the humidified air	65	°C
Contact pressure between flow field and MEA	0.78	N mm^{-2}

is between 8 and 37 μm. The reaction resistance is determined by the charge transfer resistances, R_{ct}, connected in parallel with the double layer capacitance, C_{dl}, at the phase boundary between the electrolyte and carbon supported platinum particles. The protons are formed during the methanol oxidation reaction and transported through the chains of the electrolyte membrane. In the mathematical model, the resistance due to the proton conduction in the electrolyte present in the electrode is represented by R_{pore}. Since the resistance or the potential difference to which the protons in the electrolyte are exposed depends on the distribution of the electrolyte, the effect of the spatial distribution on this resistance is considered in the chain ladder model. The resistance to proton transfer from the anode to the cathode through the electrolyte membrane is represented by R_{mem}, which denotes the ohmic resistance. Unlike the conduction of protons through the electrolyte membrane, the resistance due to the conduction of the produced electrons through the porous media is negligible.

At the anode, the complex methanol oxidation can result in the formation of various adsorbates on the platinum catalyst particles. Further, there is the need of an adsorbed OH group on the ruthenium catalyst for promoting the CO oxidation by the bifunctional mechanism. In the equivalent circuit, only the rate determining step for the adsorption/desorption-mechanism is considered to obtain the inductive arc. This behavior occurs since a potential change must first take place before a current can be drawn as the CO surface coverage changes electrochemically during this step. The adsorption/desorption-mechanism of CO is represented by:

$$CH_3OH \rightarrow CO_{ads} + OH \rightarrow CO_2 \tag{2}$$

where, depending on the potential, one of the steps in the reaction presented in Equation (2) can be rate determining. The change in rates of the coverage of other intermediates in the methanol oxidation reaction is large compared to the change in the rate of the CO surface coverage on platinum [1,2,11]. In this work, we consider the dominant elements as illustrated in Fig. 2, also see Ref. [2].

The high frequency resistance (HFR) is normally measured at a frequency of 10 kHz and is part of the membrane resistance, R_{mem} [Ω]. The 45° branch at high frequencies and the capacitive arc are simulated in ZView™ [12] as a distributed element implemented as a macro-homogenous porous electrode according to Paasch [13]:

$$Z(\omega) = \frac{\rho_{pore} d}{A} \frac{\coth\left(\sqrt{\frac{k + i\omega}{\omega_1}}\right)}{\sqrt{\frac{k + i\omega}{\omega_1}}} \quad [Z(\omega)] = \Omega \tag{3}$$

where this model is based on the chain ladder model described in Ref. [13] with ρ_{pore} as the specific resistance of the pore electrolyte, d is the thickness of the electrode, A is the geometric area of the electrode, ω is frequency of the AC signal and i is the imaginary unity. The characteristic frequency, k, is defined as the ratio of charge transfer conductance, g_{ct}, to the double layer capacitance per unit length, C_1, as follows:

$$k = \frac{g_{ct}}{C_1} = \frac{j_0 nF}{CR_g T} \quad [k] = \frac{1}{s} \tag{4}$$

where j_0 is the exchange current density, n is the number of electrons, F is the Faraday constant, C is the double layer capacitance per area, R_g is the universal gas constant and T is the temperature. The double layer capacitance per unit length is defined as $C_1 = AS_cC$ with S_c as the pore surface per unit volume where the double layer can form. Moreover:

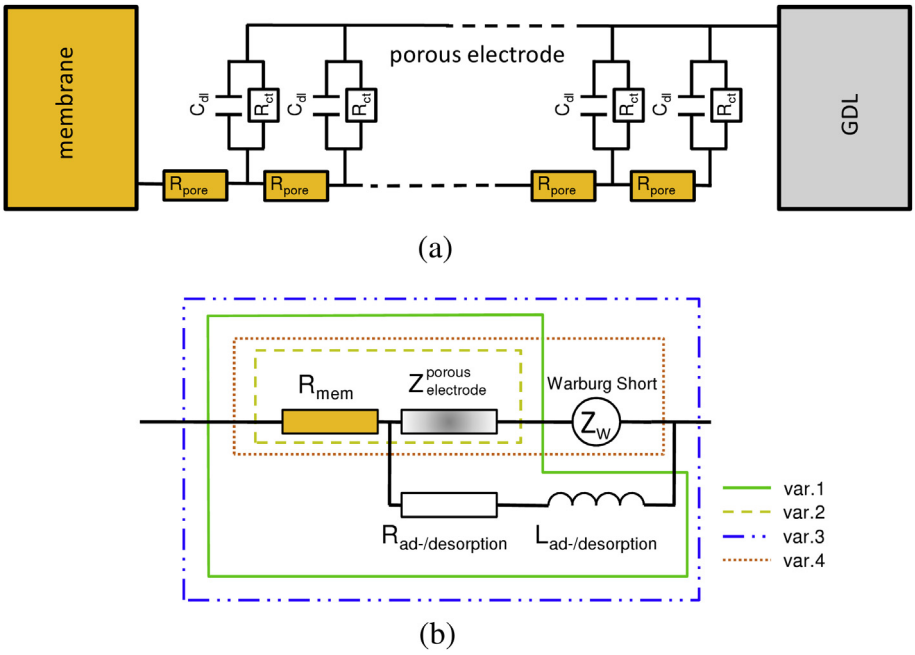

Fig. 2. (a) Simplified cylindrical pore model considered for the anode catalyst layer in this work; (b) variations used in the model of the anode spectra in ZView™ – Var. 1: small current densities, Var. 2: average current densities, Var. 3: medium/high current densities, Var. 4: large current densities.

$$\omega_1 = \frac{K}{d^2} \quad [\omega_1] = \frac{1}{s} \tag{5}$$

with the field diffusion constant, K, as:

$$K = \frac{1}{CS_c\rho_{pore}} \quad [K] = \frac{1}{s} \tag{6}$$

According to Paasch [12] and hence the implemented model in ZView™ [12], the porous electrode has three parameters k, ω_1 and $d\rho_{pore}$. These parameters make up the three physically relevant parameters, ρ_{pore} (specific pore electrolyte resistance), C (double layer capacitance per unit area) and g_{ct} (charge transfer conductance per length) with C and g_{ct} calculated as:

$$C = \frac{1}{d^2\rho_{pore}\omega_1 S_c} \quad [C] = \frac{F}{m^2} \tag{7}$$

$$g_{ct} = \frac{kA}{\omega_1 d\rho_{pore}} \quad [g_{ct}] = \frac{S}{m} \tag{8}$$

A second capacitive arc at low frequencies, depending on the MEA segment, can occur at higher current densities. This arc is associated with the mass transport of methanol diffusion in the void regions of the catalyst layer and/or the gas diffusion layer. This second capacitive arc occurs at higher current densities and is pronounced as the current increases; hence, it is an indication to its association with the diffusion limitations. At the same time, with current densities, the diffusion of methanol gains influence. In the equivalent circuit, the diffusion is modeled by a "finite length Warburg short circuit element" [12]:

$$Z_{warb}(\omega) = R_{warb}\frac{\tanh\sqrt{it\omega}}{\sqrt{it\omega}} \tag{9}$$

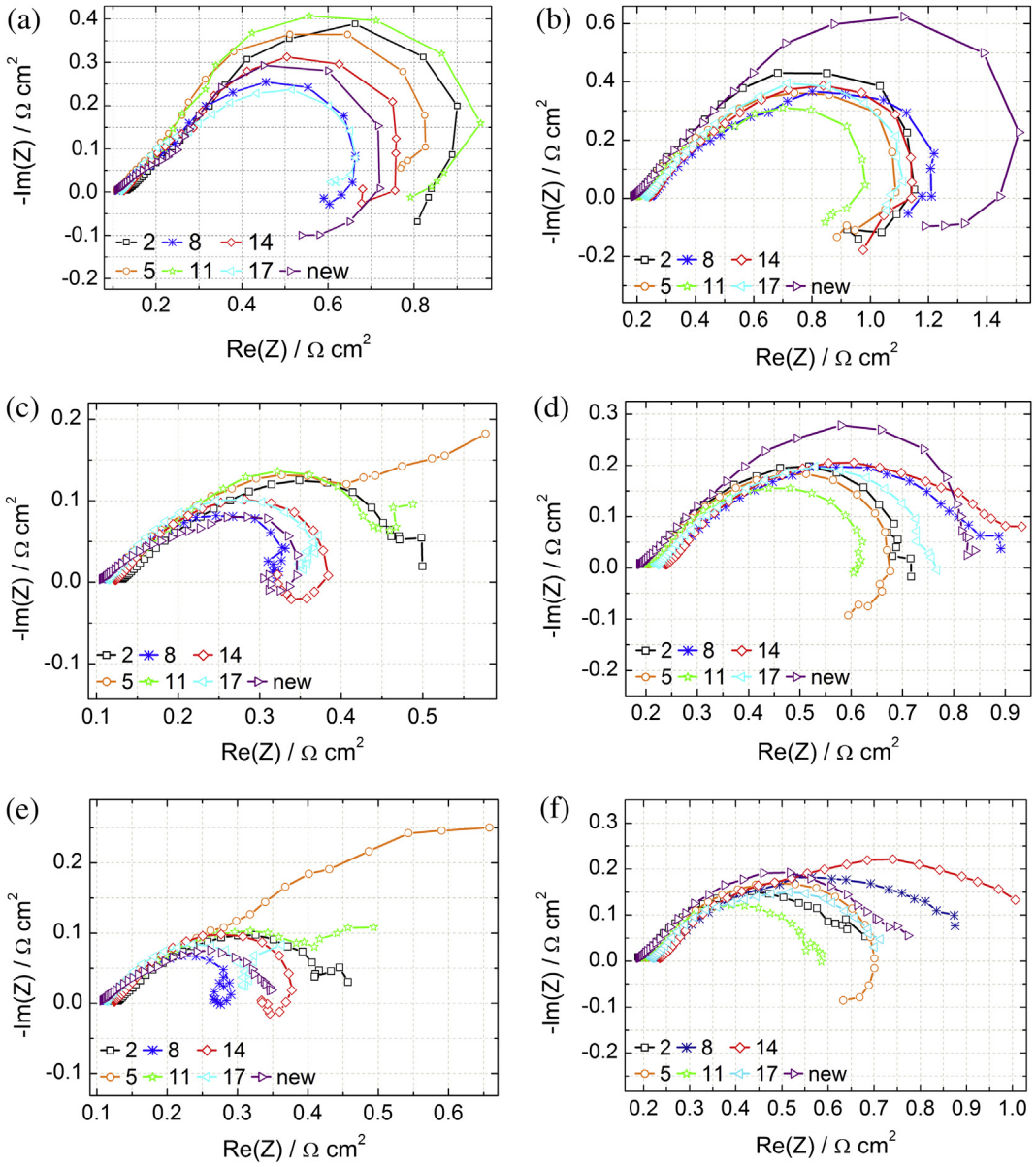

Fig. 3. Half cell spectra for all segments at various current densities (a) anode at 50 mA cm^{-2}; (b) cathode at 50 mA cm^{-2}; (c) anode at 150 mA cm^{-2}; (d) cathode at 150 mA cm^{-2}; (e) anode at 250 mA cm^{-2}; (f) cathode at 250 mA cm^{-2}.

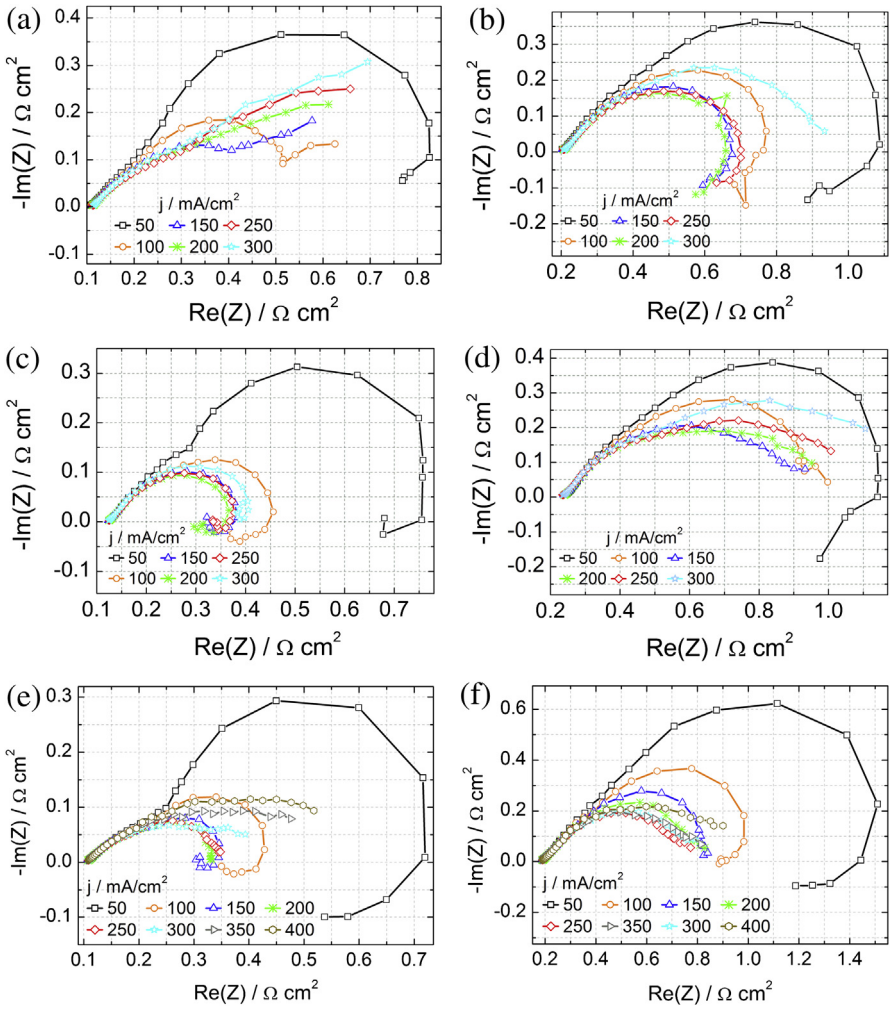

Fig. 4. Characteristic shape of the anode spectra for segments (a) 5; (c) 14; (e) new, and the cathode spectra for segments (b) 5; (d) 14; (f) new – the frequency range is 10 kHz to 0.05 Hz.

where the characteristic time constant for the diffusion process, t, is obtained as:

$$t = \frac{L^2}{D_{\text{eff}}} \quad [t] = s \tag{10}$$

In ZView™, the Warburg element is determined by considering an effective diffusion coefficient. The characteristic time constant, t, is dependent on the effective diffusion length, L, and the effective diffusion coefficient, D_{eff}. The diffusion coefficient is usually measured at low frequencies and high current densities. The inductive arc corresponding to the CO adsorption/desorption processes is modeled by a connected coil parallel to the porous electrode element, which is realized in the equivalent circuit [11]. From the equivalent circuit in Fig. 2, $R_{\text{ad/desorption}}$ represents an electro-oxidation reaction resistance of adsorbed CO and the inductance, $L_{\text{ad/desorption}}$ is an inductive element that forces a phase delay due to the slow relaxation of adsorbed CO [14].

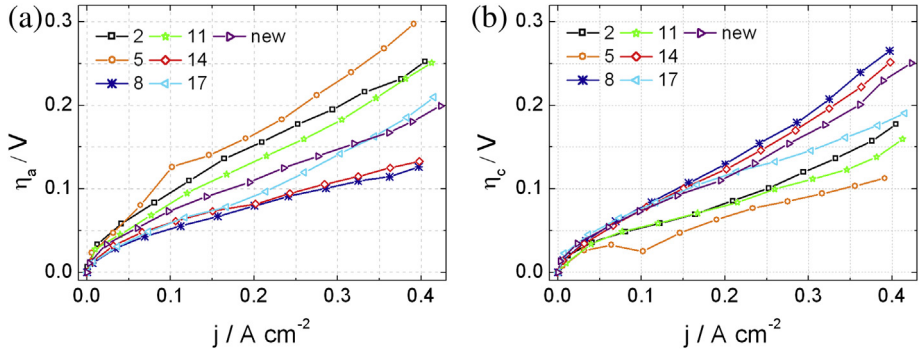

Fig. 5. (a) Anode and (b) cathode overpotential of the 6 long-term operated MEA-segments (2, 5, 8, 11, 14, 17) and the new MEA-segment [10].

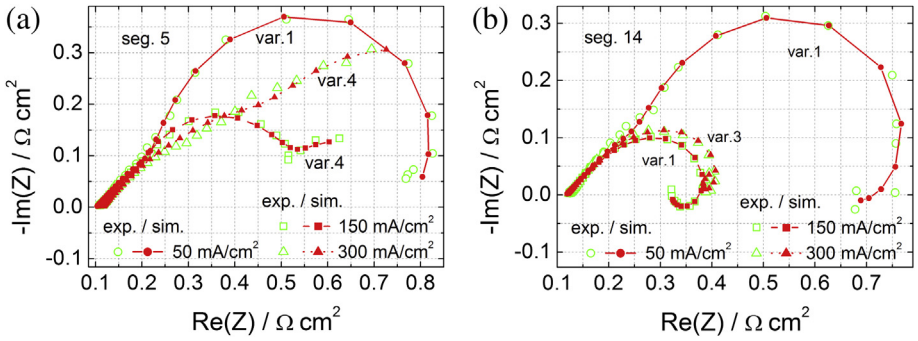

Fig. 6. Comparison between measured and calculated spectra with Var. 1 as 50 mA cm^{-2}, Var. 2150 mA cm^{-2}, Var. 3300 mA cm^{-2} – (a) segment 5; (b) segment 14.

3. Results and discussion

3.1. Experimental results

The electrochemical impedance spectroscopy in this work has been measured for various current densities from 50 to 300 mA cm^{-2} with a 50 mA cm^{-2} interval and a frequency range of 10 kHz–50 mHz. The anode and cathode spectra of the MEA segments were obtained by measuring the voltage response of both electrodes via a reference electrode arrangement, which is implemented in the cathode gas compartment. As shown in Fig. 3, the overall trend of the spectra, regardless of segment number, is similar in behavior. A 45° branch is observed at high frequencies, followed by a capacitive arc that at low frequencies, depending on current density is followed either by an inductive portion downward or a second capacitive arc. At both the anode and cathode, an overall trend of the spectra with the current density is observed. Mass transport limitations are measured with the increase of current density. However, a direct trend of the spectra from inlet to outlet of the aged MEA is not observed. A similar behavior was observed and reported in our previous analysis of this MEA [10]. Further, an independent investigation of the spectra behavior of this MEA (not reported in this paper) of randomly chosen segments over the total area of the MEA showed no clear trend from inlet to outlet.

For the sake of detailed comparison of the behavior of the spectra depending on position, we discuss the spectra measured for segments 5 and 14 of the aged MEA in more detail as shown in Fig. 4. The anode spectra of the aged MEA segment 5 are all in the first quadrant as shown in Fig. 4a. For a current density of 50 mA cm^{-2} and at low frequencies an inductive influence is recorded, while for $j \geq 100$ mA cm^{-2} a second capacitive arc is visible. This behavior could be attributed to the behavior of the anode overpotential at this segment, which is the highest of all segments as given in Fig. 5. Toward the methanol inlet, segment 14, the anode spectra of the aged MEA show an inductive effect at low frequencies for all current densities except for 300 mA cm^{-2}, where the spectrum remains in the first quadrant and at low frequencies a closed loop is observed; see Fig. 4c. The spectra of the new anode MEA show an inductive loop for a current density up to 150 mA cm^{-2}. At current densities $j \geq 200$ mA cm^{-2} the anode spectra are completely in the first quadrant as shown in Fig. 4e. This behavior is also similar with the cathode spectra; see Fig. 4f. The spectra at high current densities are open; indicating the presence of a second capacitive arc. The overpotential of the anode of the new MEA is located in the central region of the measured values.

Table 2
Dependence of the equivalent circuit model of the anode spectra used in ZView™ on the current density and the MEA-segment.

Current density in mA cm^{-2}								
MEA-segment	50	100	150	200	250	300	350	400
New	Var. 1	Var. 1	Var. 1	Var. 2	Var. 4	Var. 4	Var. 4	Var. 4
2	Var. 1	Var. 1	Var. 4	Var. 4	Var. 4	Var. 4	Var. 4	N/A
5	Var. 1	Var. 4	Var. 4	Var. 4	Var. 4	Var. 4	N/A	N/A
8	Var. 1	Var. 1	Var. 3	Var. 3	Var. 3	Var. 3	Var. 3	N/A
11	Var. 1	Var. 1	Var. 4	Var. 4	Var. 4	Var. 4	Var. 4	N/A
14	Var. 1	Var. 1	Var. 1	Var. 1	Var. 1	Var. 3	N/A	N/A
17	Var. 1	Var. 2	Var. 2	Var. 4	Var. 4	Var. 4	Var. 4	N/A

3.2. Simulated results

Simulation of the electrochemical spectra of the anode is necessary to gain further insight into the concurrent physical and chemical processes. This is established with the help of an electrical equivalent circuit, Fig. 2, created in ZView™. To establish the validity of this circuit, the experimental measurements are compared to the resultant numerical values and show very good agreement as shown in Fig. 6. In this study, this equivalent circuit is used to calculate various parameters to aid with the analysis; g_{ct}, ρ_{pore}, C_{dl}, R_{warb}, R_{coil} and L. As discussed earlier in the modeling section, each parameter can be linked to a specific phenomenon. Table 2 gives an overview of the variation of the equivalent circuit for the respective MEA segments and the corresponding current intensity used.

First, the activity of the anode catalyst layer in terms of the MOR and the level of its degradation were estimated by calculating the conductance of the charge transfer, g_{ct}, of all aged MEA segments and the new MEA as plotted in Fig. 7. An increase in this property in terms of the current density was measured, which is mainly attributed to the higher overpotential; indicating that the reaction

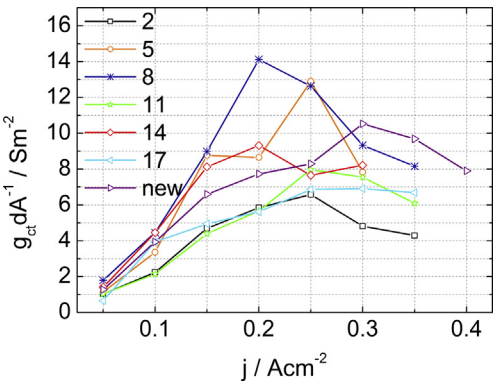

Fig. 7. The dependence of the conductance of the charge transfer on current density for all segments.

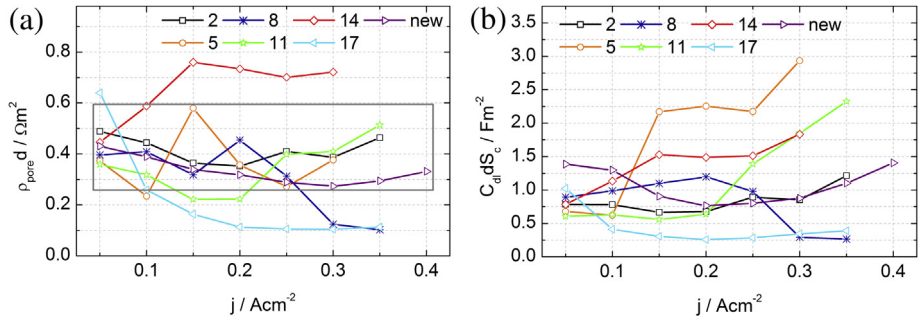

Fig. 8. (a) Specific pore electrolyte resistivity; (b) double layer capacitance in the anode and for various current densities.

takes place more quickly. However, g_{ct} reached a maximum and decreased afterward. This behavior is not expected in terms of a simple one-step reaction mechanism. Hence, it is suggested that the conductance of the charge transfer calculated in this study is of that of a multi-step complex methanol oxidation. Here, the rate-limiting step in the MOR is not necessarily the charge transfer reaction of the oxidizing methanol to CO, but rather it can also be due to an insufficient oxidation of CO to CO_2 via provided OH groups [15]. This oxidation, however, might not be fast enough, leading to a decreasing number of available Pt sites for the oxidation of methanol. Therefore, the conductance of the charge transfer g_{ct} decreases with increasing current at high current density values. Segment 8 shows the best overall value of g_{ct}, which is recorded at a current density of 0.2 A cm^{-2}. The g_{ct} of the new MEA lies between that of the aged segments. However, compared to the aged MEA segments, a drop in the g_{ct} value of the new MEA occurs at a higher current density (>0.3 A cm^{-2}) and the overall drop is much lower, which results in the highest g_{ct} at 0.3 and 0.35 A cm^{-2} for the new MEA. This suggests that the new MEA has the highest Ru content providing the −OH groups for a fast oxidation of CO to CO_2. Further, enough platinum particles are available for the MOR to occur. But in all cases, for the new and degraded MEAs, at high current densities the bi-functional mechanism for the MOR seems not to be sufficient. The loss of Ru in the aged MEA segments has been examined in our previous work [10] using EDX analysis and confirms this result.

The second parameter, which is of significance, is the specific pore electrolyte resistivity, ρ_{pore}. As shown in Fig. 8a, this parameter, with the exception of segments 17 and 14, is independent of location and lie in a relatively narrow range for all current densities. This is expected as this parameter is strongly influenced by the water content of the pore electrolyte, the ionomer content and its distribution in the electrode. At the anode, the water content of the ionomer in the electrode should be at optimum for all segments as a water–methanol solution is used as fuel. Drying out of the pore electrolyte in a similar manner as at the anode of a hydrogen polymer electrolyte membrane fuel cell via the transport of ions in water molecules to the cathode is unlikely [16].

The porous electrode is further investigated by calculating the double layer capacitance, C_{dl}; plotted in Fig. 8b. The overall trend is an increase of the double layer capacitance with current density for nearly all the segments. This might be attributed to the direct relationship of the double layer capacitance to the operation point and the degree of surface coverage by adsorbed intermediates, such as $MeOH_{ads}$, CO_{ads}, COH_{ads} and OH_{ads}. With increasing anode potential, i.e. increasing current density, the coverage should decrease, which might be an explanation of the changing capacity.

Next, transport limitations due to diffusion were investigated by estimating the diffusion resistance R_{warb}, defined as the limit of the Warburg impedance for $\omega \rightarrow 0$. This diffusion limit is found to increase with the current density for nearly all segments as shown in Fig. 9a. From this figure, recalling the spectra of the anode, the diffusion loop measured in the spectra can be correlated to the diffusion limitations identified by the diffusion resistance at high current densities. As illustrated R_{warb} of the new MEA shows the lowest degree of limitation toward diffusion; correlating to no diffusion loop in the segment's spectrum. Further, the diffusion resistance can also be quantified by the diffusion coefficient. This parameter can be estimated for the various segments using Equation (10) and shows no uniform trend as shown in Fig. 9b. As expected, the diffusion is much faster in the new MEA than in the aged MEA segments.

Using the R_{warb}, the diffusion processes and the transport limitations associated with it can be further investigated. Taking into account the tortuosity of the electrode and the fluctuating thickness of the catalyst layer on the anode side between 8 and 30 μm, we use an effective diffusion length of 60 μm; hence, resulting from the model parameters t, the effective diffusion coefficient is:

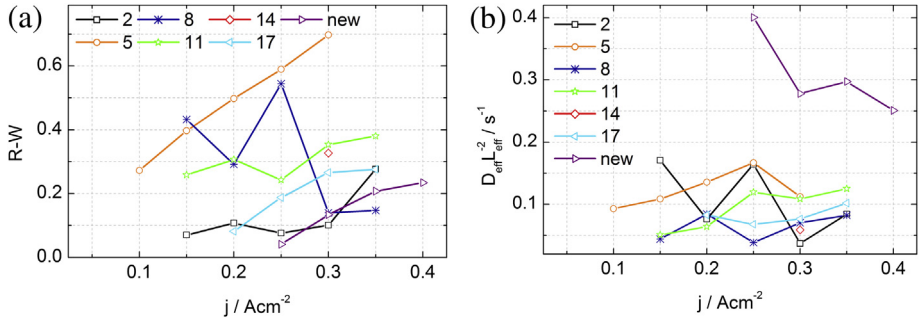

Fig. 9. (a) Diffusion resistance R–W; (b) effective diffusion coefficient in the anode catalyst layer and for various current densities.

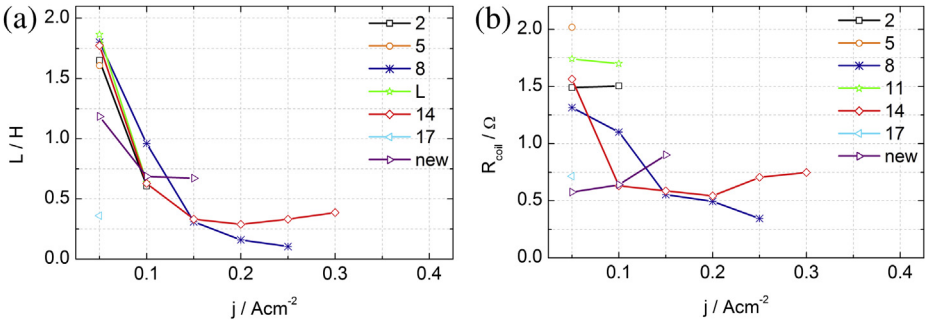

Fig. 10. (a) Pseudo-inductance; (b) ohmic resistance of the pseudo-inductance for the anode catalyst layer and various current densities.

$$D_{\text{eff}}^{\text{An,old}} = \frac{L_{\text{eff}}^2}{t} \approx \frac{60\ \mu\text{m}^2}{0.08\ \text{s}} = 2.88 \times 10^{-10}\ \text{m}^2\ \text{s}^{-1} \tag{11}$$

$$D_{\text{eff}}^{\text{An,new}} = \frac{L_{\text{eff}}^2}{t} \approx \frac{60\ \mu\text{m}^2}{0.26\ \text{s}} = 9.36 \times 10^{-10}\ \text{m}^2\ \text{s}^{-1} \tag{12}$$

The effective diffusion coefficient of methanol in the pore phases of the GDL is dependent on temperature as follows [17]:

$$D_{\text{MeOH,eff}}^{\text{An,GDL}} = 0.7 \cdot 10^{(-1.4163 - 999.778/T)} \times 10^4\ \text{cm}^2\ \text{s}^{-1} \tag{13}$$

where for a temperature of 343 K, the diffusion coefficient is $3.3 \times 10^{-5}\ \text{m}^2\ \text{s}^{-1}$.

The effective diffusion coefficient of methanol in the anode catalyst layer can be calculated by Ref. [18]:

$$D_{\text{MeOH,eff}}^{\text{An,CL}} = \left(1 - \varepsilon_{\text{s}}^{\text{ac}} - \varepsilon_{\text{m}}^{\text{ac}}\right)^{1.5} D_{\text{MeOH,H}_2\text{O}} \quad \text{m}^2\ \text{s}^{-1} \tag{14}$$

where $D_{\text{MeOH,eff}}^{\text{An,CL}}$ is the effective diffusion coefficient of methanol in the anode catalyst layer, $\varepsilon_{\text{s}}^{\text{ac}}$ is the solid fraction in the catalyst layer, $\varepsilon_{\text{m}}^{\text{ac}}$ is the fraction of electrolyte membrane in the layer and $D_{\text{MeOH,H}_2\text{O}}$ is the binary diffusion coefficient of methanol in water. Using $\varepsilon_{\text{s}}^{\text{ac}} = 0.6$, $\varepsilon_{\text{m}}^{\text{ac}} = 0.08$ and $D_{\text{MeOH,H}_2\text{O}} = 1.93 \times 10^{-9}\ \text{m}^2\ \text{s}$, the diffusion coefficient of methanol in the catalyst layer is obtained as $D_{\text{MeOH,eff}}^{\text{An,CL}} = 3.5 \times 10^{-10}\ \text{m}^2\ \text{s}^{-1}$. From the model parameters, the effective diffusion coefficient is calculated in the order of magnitude of the effective diffusion coefficient of the methanol in the catalyst layer. Hence, the detected diffusion process is most probably occurring as the diffusion of CH_3OH in the pores of the catalyst layer rather than the GDL.

Finally, the degree of the poisoning of the platinum catalysts can be estimated by two parameters: (1) the coverage of CO, θ_{CO}, which is investigated via the calculation of the parameter L and (2) R_{coil}, which monitors the effects of the phase shift between the voltage and current corresponding to the reaction process [1]. From Fig. 10, it can be seen that L decreases with an increasing current. A pseudo inductive behavior of the current density, or the potential, of the anode indicates that this is a phenomenon of the kinetics of methanol oxidation. The parameter L is estimated to have a much more prolonged change with current density for the aged MEA segments 8 and 14. This shows that CO_{ads} has an influence on the cell behavior even at relatively high anode potentials. This is inline with other measurements in which dominance of the kinetic problem is found in segments 8 and 14, while the diffusion dominance is measured for segment 5 only at $j = 50\ \text{mA cm}^{-2}$ (as illustrated from the inductive behavior in the EIS measurements). The measurements and simulation results indicate that at segments 8 and 14 there is a lack of oxygen adsorbates since not enough active Ru particles are available. Consequently, the oxidation of CO to CO_2 on the Pt particles at lower potentials is no longer possible.

4. Conclusions

In this study, the electrochemical impedance spectroscopy technique was used to investigate the degradation of an aged direct methanol fuel cell MEA experimentally and numerically. To further our understanding of localized degradation, the cathode and anode spectra were collected for various segments along the methanol flow field. A specific trend in the performance from methanol inlet to outlet was not found; keeping in line with our findings in Ref. [10]. The cathode spectra exhibited an inductive influence at high current densities, while a contrasting behavior in the anode spectra was observed. Further investigation of the anode spectra via an equivalent circuit revealed that at high current densities the methanol oxidation following the bi-functional mechanism is limited by the oxidation of CO to CO_2 via provided OH groups. This equivalent circuit was also used to calculate the effects of proton transport in the catalyst layer and transport limitations due to methanol diffusion in the anode catalyst layer. Mass transport limitations in the anode were significant at these currents. Finally, CO poisoning of the platinum catalyst was investigated in the terms of CO coverage. The adsorption of carbon monoxide was found to have an influence on the cell behavior even at relatively high anode potentials.

Acknowledgments

This work was financially supported by the “Bundesministerium für Wirtschaft und Technologie” under contract 0327853B. We would also like to acknowledge our cooperation partners Dr. K. Wippermann and J. Mergel from FZ Jülich for the supply of the MEA samples. The author N. Zamel would like to acknowledge the financial support by the Natural Sciences and Engineering Research Council of Canada (NSERC) in the form of a Postdoctoral Fellowship.

References

[1] J.T. Müller, P.M. Urban, W.F. Hölderich, J. Power Sources 84 (1999) 157–160.
[2] F. Seland, R. Tunold, D.A. Harrington, Electrochim. Acta 51 (2006) 3840–3872.
[3] N.Y. Hsu, S.C. Yn, K.T. Jeng, C.C. Chien, J. Power Sources 161 (2006) 232–239.
[4] S. Uhm, S.T. Chung, J. Lee, J. Power Sources 178 (2008) 34–43.
[5] T. Schulz, C. Weinmüller, M. Nabavi, D. Poulikakos, J. Power Sources 195 (2010) 7548–7558.
[6] J.Y. Park, J.H. Lee, J. Sauk, I.H. Son, Int. J. Hydrogen Energy 33 (2008) 4833–4843.
[7] W. Vielstich, A. Lamm, H.A. Gasteiger, Handbook of Fuel Cells Fundamentals Technology and Applications, in: Electrocatalysis, Part 3, vol. 2, Wiley, 2003.
[8] X.Z. Yuan, C. Song, H. Wang, J. Zhang, Electrochemical Impedance Spectroscopy in PEM Fuel Cells Fundamentals and Applications, Springer, 2010.
[9] D. Gerteisen, J. Appl. Electrochem. 37 (2007) 1447–1454.
[10] P. Hartmann, D. Gerteisen, J. Power Sources 219 (2012) 147–154.

[11] J.R. Macdonald, E. Barsoukov, Impedance spectroscopy: theory, experimental and applications, in: N. Wagner (Ed.), Fuel Cells, second ed., 2005 Chapter 4.5.4.
[12] ZView™. ZView™ impedance/gain phase, graphing and analysis software: User Manual, Version 3.2. Scribner Associates, Inc. 150 East Connecticut Avenue, Southern Pines, NC 28387, Revised 11/2010.
[13] G. Paasch, K. Micka, P. Gersdorf, Electrochim. Acta 38 (1993) 2654–2662.
[14] M.K. Jeon, J.Y. Won, K.S. Oh, K.R. Lee, S.I. Woo, Electrochim. Acta 53 (2007) 447–452.
[15] A. Havranek, Relationship Between Structure and Electrochemical Properties of Direct Methanol Fuel Cell Anodes. Dissertation, Rheinisch-Westfällsche Technische Hochshule RWTH, Aachen, 2005.
[16] B.H. Andreaus, Die Polymer-Elektrolyt Brennstoffzelle – Charakterisierung ausgewählter Phänomene durch elektrochemische Impedanzspektroskopie. Dissertation, EPFL Nr2598, Ecole Polytechnique Federale de Lausanne, 2002.
[17] A. Casalegno, R. Marchhesi, D. Parenti, Fuel Cells 8 (2008) 37–44.
[18] C.H. Chen, T.K. Yek, J. Power Sources 160 (2006) 1131–1141.